

# Diameters of Mira Stars Measured Simultaneously in the J,H,K' Near-Infrared Bands

R. Millan-Gabet<sup>1</sup>, E. Pedretti<sup>2,6</sup>, J. D. Monnier<sup>2</sup>, F. P. Schloerb<sup>3</sup>, W. A. Traub<sup>4</sup>, N. P. Carleton<sup>4</sup>, M. G. Lacasse<sup>4</sup> and D. Segransan<sup>5</sup>

rafael@ipac.caltech.edu

## ABSTRACT

We present the first spatially resolved observations of a sample of 23 Mira stars simultaneously measured in the near-infrared J, H and K' bands. The technique used was optical long baseline interferometry, and we present for each star visibility amplitude measurements as a function of wavelength. We also present characteristic sizes at each spectral band, obtained by fitting the measured visibilities to a simple uniform disk model. This approach reveals the general relation J diameter < H diameter < K' diameter.

*Subject headings:* stars: atmospheres, fundamental parameters, variables — instrumentation: interferometers — techniques: high angular resolution

## 1. Introduction

Mira stars are variable, pulsating stars in the asymptotic giant branch (AGB). They have pulsation periods of about 100 – 1000 days, during which their light curves exhibit large amplitude variations (as high as 10 magnitudes at visual wavelengths, becoming a

---

<sup>1</sup>Michelson Science Center, California Institute of Technology, Pasadena, CA 91125, USA

<sup>2</sup>University of Michigan, Astronomy Department, Ann Arbor, MI 48109, USA

<sup>3</sup>University of Massachusetts at Amherst, Astronomy Department, Amherst, MA 01003, USA

<sup>4</sup>Harvard-Smithsonian Center for Astrophysics, Cambridge, MA 02138, USA

<sup>5</sup>Observatoire de Genève, Switzerland

<sup>6</sup>NASA Michelson postdoctoral fellow

more modest  $\sim 1$  mag in the near-infrared), and their spectral types vary by a few subclasses. During the pulsation cycle, their photospheric radii are thought to vary by 5–50 %. Mira star atmospheres are geometrically extended and have very low effective temperatures ( $\lesssim 3000$  K), hence they are a rich molecular composition. They exhibit high mass loss rates (a few  $10^{-6} M_{\odot}/yr$ ), and the ejected material forms layers which become sites of circumstellar maser activity and dust formation. Thus, although the Mira evolutionary stage is relatively short ( $\sim 5 \times 10^5$  yrs), it is a crucial one in order to understand a variety of phenomena such as high mass loss, the formation of planetary nebulae, and the chemical enrichment of the galaxy.

Despite the existing large body of observational and theoretical work, many aspects of the physics of Mira stars remain poorly understood; in particular their detailed atmospheric stratification and composition, and their dominant mode of pulsation. This is to a large extent a consequence of their intrinsic complexity (treatment of 3D convection, photospheric shocks, and rich photospheric chemistry), and most needed are new observational data that can help discriminate between the large number of theoretical models that have been proposed.

Spatially resolved observations of Mira stars are clearly desirable, and can be easily obtained using high resolution techniques such as long baseline interferometry. The geometrically extended and chemically rich nature of Mira star atmospheres manifests itself in apparent physical sizes which depend on the wavelength of observation, especially when crossing regions in the spectrum where the opacity changes rapidly. This fact was first observed in the visible region of the spectrum, where sizes as much as 50% smaller are found in narrowband near-continuum filters than in filters contaminated by TiO absorption (Bonneau & Labeyrie 1973; Labeyrie et al. 1977; Bonneau et al. 1982; Haniff, Scholz & Tuthill 1995; Hofmann et al. 2000, 2001).

Although originally expected to be better probes of the underlying stellar continuum, measurements at infrared wavelengths also exhibit non-trivial wavelength dependence. Synthesizing measurements obtained at different facilities, it appears that as a general trend, Mira sizes appear large in the visible (Tuthill et al. 1994; Haniff, Scholz & Tuthill 1995; Ireland et al. 2004), smaller in the near-infrared (Perrin et al. 1999; Hofmann et al. 2002; van Belle, Thompson & Creech-Eakman 2002, and references therein), and larger again at thermal infrared wavelengths (Mennesson et al. 2002; Weiner, Hale & Townes 2003a,b). The interpretation of this broad trend is that the outer layers (i.e. those layers above a level that could be called “the photosphere”) are relatively obscure in the visible, relatively transparent in the near-infrared, and again relatively obscuring in the thermal infrared. The physical basis for this variation of opacity with wavelength can be modelled once the underlying em-

prical variation of diameters with wavelength is established by observations. The purpose of this paper is to show that there is such a variation through the near-infrared, as defined by the J, H and K' bands.

Due to instrumental limitations, *simultaneous* measurements at different wavelengths are scarce in the literature, but are clearly the optimum way to explore the wavelength-dependent structure, since Mira stars are suspected of exhibiting important cycle-to-cycle non-repeatability. Dramatic size increases (25 – 100%) have been observed between near ( $\sim 1.1 - 2.3\mu m$ ) and thermal ( $\sim 3.1 - 3.8\mu m$ ) infrared measurements, both in narrow (Tuthill, Monnier & Danchi 2000; Tuthill et al. 2000) and broad bands (Mennesson et al. 2002). Smaller but significant (1–20%) effects have been observed in narrow bands within the near-infrared K-band ( $\sim 2.0 - 2.4\mu m$ ), as the narrow filters preferentially sample portions of the spectrum corresponding to strong molecular bands or the adjacent continuum (Thompson 2002; Thompson, Creech-Eakman & van Belle 2002; Perrin et al. 2004). Using the same portion of the spectrum as in this work, Weigelt et al. (2003) studied the visibility of the Mira star T Cep dispersed across the J/H/K bands, finding similar J and H sizes which are  $\sim 10\%$  smaller than the K-band size; as well as size differences within the K-band as large as 26%.

Clearly, the richness of the size-wavelength relation holds the potential to be the best probes of atmospheric structure in these stars. In turn, as has been illustrated in the recent multi-wavelength modelling effort by Perrin et al. (2004), a complete model that includes the stellar photosphere, dominant opacity sources and possible additional emitting layers must be globally fit in order to also extract accurate stellar diameters, and derive conclusions about the pulsation mode.

In this paper we present the first systematic survey of Mira star diameters measured near-simultaneously in the near-infrared J, H and K' bands. This new multi-color data set allows us in particular to derive apparent size ratios, which are immune to many sources of calibration error. In § 2 we describe the measurement technique and Mira sample observed; in § 3 we describe the data analysis procedure; in § 4 we present our results, both in the form of uniform diameter fits at each spectral band in order to illustrate the main trends in these wavelength regions, and as tables of calibrated visibility data for straightforward use in global fitting including other datasets; in § 5 we discuss our main results and places them in context of recent theoretical work.

## 2. Observations

Observations were carried out at the Infrared-Optical Telescope Array (IOTA), a long baseline interferometer located on Mount Hopkins, AZ (see e.g. Traub 1998). The data presented here were obtained using the two telescopes available at the time, on two configurations which provide physical baseline lengths of approximately 21 m and 38 m, at geographic azimuth angles (measured East of North) of  $-4$  deg and  $+18$  deg respectively.

The beam combination and fringe detection instrumentation is exactly as described in Millan-Gabet (1999) and Millan-Gabet et al. (2001). In short, afocal telescope beams were combined at a bulk optics beam combiner, and interferograms were produced by modulating the optical path difference (OPD) between the two beams by  $\pm 60\mu m$ . The fringe modulation frequencies are in the range 100 – 2000 Hz, chosen as an optimum trade-off between maximizing the photon signal and minimizing the readout time to freeze out atmospherically induced OPD variations during the fringe acquisition. The two outputs of the beam splitter were focused on two well-separated pixels of a NICMOS3 array, the readout of which is synchronized with the optical path modulation (Millan-Gabet et al. 1999).

The NICMOS3 camera contains a set of three standard near-infrared J ( $\lambda_0 = 1.25\mu m$ ,  $\Delta\lambda = 0.28\mu m$ ), H ( $\lambda_0 = 1.65\mu m$ ,  $\Delta\lambda = 0.30\mu m$ ) and K' ( $\lambda_0 = 2.16\mu m$ ,  $\Delta\lambda = 0.32\mu m$ ) filters, where ( $\lambda_0$ ,  $\Delta\lambda$ ) are the center wavelength and full-width at half-maximum respectively. Rapid switching between the three filters guaranteed near-simultaneous observations (within a few minutes) in the three bands.

A typical observation consisted of 500 interferograms, obtained in a few minutes, followed by a measurement of the sky background. Target observations are interleaved with an identical sequence obtained on calibrator stars which are unresolved by the interferometer or have small diameters which can be estimated. This sequence was repeated for each of the three filters.

The basic properties of the Mira stars observed are listed in Table 1, and a log of observations is given in Table 2.

## 3. Data Analysis and Validation

The data reduction and calibration procedures are also essentially as described in Millan-Gabet (1999) and Millan-Gabet et al. (2001). For each interferogram, a peak fringe visibility (the fringe amplitude relative to the mean flux detected) is estimated by (a) correcting the intrinsic detector non-linearity, (b) sky subtraction, (c) subtracting the normalized outputs

of the beam splitter, to enhance the SNR, and (d) fitting the central three fringes of the resulting interferograms in the time domain to a point source response template computed as the Fourier transform of the spectral bandpass used in the observation.

As a result of the fringe fitting procedure, we obtain the following quantities for each interferogram: mean, fringe amplitude, position of the central fringe, and sampling rate. The data are flagged as being a false fringe identification if an individual fringe visibility is outside the range  $0.0 - 1.0$ , or if either the central fringe position or sampling rate has a value which is more than three times the standard deviation obtained from the ensemble of the 500 reduced interferograms in the observation. Finally, an entire observation is rejected if the standard deviation of the central fringe position values exceeds  $L/2$ , where  $L = 120 \mu\text{m}$  is the OPD sweep for each interferogram.

For each observation, the above procedure results in several hundred estimates of the fringe visibility, one per interferogram that survives the flagging procedure. A final estimate for the observation is formed as the mean of those values, with an internal statistical error given by the error in the mean.

Calibrator stars are measured close in space and time to the target observations in order to estimate the instrument’s system visibility. Calibrated visibility amplitudes are obtained by dividing the target visibilities by estimates of the system visibility at the time of the target observations formed by spline interpolation of the calibrator observations. A correction to the system visibility resulting from the finite but known size of the calibrator stars is applied. Standard error propagation is used to include in the calibrated visibility the error resulting from the division by the system visibility and the systematic error resulting from the uncertainty in the calibrator star sizes.

The calibrator sizes and uncertainties are in Table 3; these values were estimated as follows: (1) if available, adopt a near-infrared direct measurement from the CHARM catalog (Richichi & Percheron 2002); or else (2) if available, adopt the value based on stellar atmosphere modelling of Borde et al. (2002) or Cohen et al. (1999); or else (3) if available, and if the star is a luminosity class I, II, or III, use the empirical size-color relations of van Belle (1999); or else (4) fit the available visual and infrared photometry with a stellar blackbody model, using the *Fbol* module of the *getCal* software <sup>1</sup>.

In order to obtain characteristic sizes at each wavelength, the calibrated visibility data obtained at each spectral band were fit using a simple uniform disk (UD) model for the stellar

---

<sup>1</sup>*getCal* is a software package for planning of interferometer observations produced by the Michelson Science Center at the California Institute of Technology (<http://msc.caltech.edu/software/index.html>)

brightness. Although it is well known that for Mira stars the UD is in most cases not a good representation of the true center-to-limb variation (CLV), reconstruction of the true CLV is not possible when only sparsely sampled visibility data are available. In near-continuum bandpasses however, as near-infrared filters are to a large extent, UD profiles are expected to approximate the CLV better than at other wavelengths (Scholz 2003). Moreover, all the visibility data presented here were obtained at spatial frequencies well inside the first lobe of the visibility function (except for one star, R Leo, as discussed in § 4), where departures from the UD intensity profile are virtually undistinguishable, and therefore baseline dependent errors are expected to be minimal in this dataset.

In Figure 1, we show 4 representative examples (out of a total of 34 similar observations) of the data and fitting results. The examples are chosen to illustrate distinct aspects of the data. The top two panels illustrate the general trend found that J diameter < H diameter < K' diameter. The bottom left panel illustrates our ability to sample relatively low visibilities for bright sources. The bottom right panel shows an example where Earth rotation allowed sampling of a relatively large range of projected baseline length, illustrating the visibility data precision for observations within a single night; here the visibility fit RMS is 0.01, or 3.8% of the (changing) model visibility, which is a typical value for the dataset (full range is 1–10%).

The night-to-night data consistency was evaluated by comparing the results obtained when the same star was observed on different nights, at similar pulsational phase and using the same baseline, in order to isolate the test from possible size variations and non-circular star shapes. There are 3 such cases in our dataset ( $\times 3$  bands for a total of 9 independent comparisons) and the result is that the night-to-night consistency in visibility is in all cases better than 8%, with mean values being 2.3%, 3.0% and 3.8% for J, H and K' respectively.

Our data can also be compared with previous measurements from the literature. This comparison can only be made at K-band. Considering the most recent measurements (Perrin et al. 1999; van Belle, Thompson & Creech-Eakman 2002; Monnier et al. 2004) we find that (a) our diameters show no systematic positive or negative bias with respect to the literature values, and (b) the diameter values agree to 20% or better. Considering that no effort was made to compare data taken only at similar pulsational phases, this level of agreement appears reasonable, given for example that K-band Mira sizes can change by 10% for a phase difference of only 0.04 (Perrin et al. 1999).

## 4. Results

Recognizing that potentially the best use of our J/H/K' measurements will be as part of a larger modelling effort which incorporates for each star all the available data across the spectrum, a goal beyond the scope of this paper, we provide in Table 4 the totality of our visibility measurements. Columns 1 – 4 give the star name, calendar/Julian observation epoch, and filters used. Columns 5 – 7 give the 2-dimensional spatial frequencies ( $u, v$ ), and measured visibilities.

In addition, in order to capture the essential features of the “size” – wavelength relation across the near-infrared, we provide in Table 5 the results of fitting our visibility data to UD models. Columns 1 – 4 give the star name, observation Julian date, the pulsation phase<sup>2</sup> and an estimate of the spectral type for that pulsation phase (see § 5). Columns 5 – 7 give the J, H and K'-band best fit UD diameters. The fact that we have measurements at 3 different wavelengths, allows us to make a relative measurement in terms of diameter *ratios*, given in columns 8 – 9, which are expected to be immune to some sources of systematic error (e.g. calibrator diameter uncertainty, seeing effects) and also represent the linear size ratios independent of (uncertain) distances.

For R Leo, essentially a single spatial frequency was sampled at H and K' bands, and the visibilities are sufficiently low that mathematically, three solutions to the UD fit exist: one in the main lobe of the visibility function, and two in the second lobe. We therefore use apriori knowledge of R Leo's nominal near-infrared size to further constrain our solutions. For K'-band, we use the diameter measured by Monnier et al. (2004) ( $30.3 \pm 0.2$  mas) as a starting value for the fit. For H-band, we use the unpublished value obtained by one of us (J. D. Monnier) from aperture masking at the Keck telescope ( $\sim 30$  mas), to obtain the two first lobe solutions indicated in Table 5. Without spatial frequency coverage that follows the shape of the visibility function, it is not possible to discriminate between these solutions, and therefore we have dropped this star from the analysis that follows.

As is apparent in Table 5, the basic result of this paper is that the near-infrared diameters are found to follow the trend: J diameter < H diameter < K' diameter. This result is also illustrated in Figure 2, where the angular diameter ratios are plotted as a function of pulsation phase. The mean values of the diameter ratios are:

---

<sup>2</sup>For each observation we have estimated the pulsation phase at the observation epoch as follows. The AFOEV (<http://cdsweb.u-strasbg.fr/afoev/>) and AAVSO (<http://www.aavso.org/>) databases were used to obtain the epochs of maximum light before and after the IOTA observation,  $o_{max1}$  and  $o_{max2}$  respectively. The phase at the IOTA epoch is then estimated as  $\text{Phase} = (\text{IOTA epoch} - o_{max1}) / (o_{max2} - o_{max1})$ .

$$\begin{aligned} \overline{R_{J/H}} &= 0.93 \pm 0.02 \\ \overline{R_{H/K'}} &= 0.89 \pm 0.02 \end{aligned} \tag{1}$$

where the  $1 - \sigma$  uncertainty is given by the error in the mean, and the (sample RMS, number of observations) are (0.09,16) and (0.09,24) for J/H and H/K' respectively.

We finally comment on a few cases for which there are intriguing changes in the measured sizes, above the levels of calibration accuracy demonstrated in § 3. As can be seen in Table 5, whenever there is both a significant time difference between two epochs of observation and the baselines used were different, apparent size changes in the range 10 – 30% can occur (R Aur, U Ori, R Lmi, S Crb, R Ser). Given the variety of possible effects at play however (physical changes in the stars, inadequacy of the UD model, stellar asymmetries probed for different baseline orientations), it is difficult to assess whether these effects are real or arise from unusually high calibration errors. These issues might be resolved with further observations.

## 5. Discussion

We have measured the diameters of 23 Mira stars simultaneously in the near-continuum near-infrared J, H and K' bands, a first for each star in the sample. The simultaneity of the measurements guarantees that the same physical state of the star is measured in each band. We find the apparent size relation: J diameter < H diameter < K' diameter, in agreement with expectations that the shorter near-infrared filter (J-band) better samples the true photospheric continuum, and that the H and K' filters contain progressively more opacity contamination from molecules in higher layers (see e.g. Jacob & Scholz 2002). In terms of the magnitude of the size difference, or diameter ratios, we find that the stars appear to be as much as 24% smaller at J than at H (mean 8%) and as much as 27% smaller at H than at K' (mean 11%). These magnitudes are in general agreement with the models of Jacob & Scholz (2002) and Ireland, Scholz & Wood (2004); although clearly detailed comparisons must be made for specific stars and specific models.

Changes in the near-infrared sizes of individual Mira stars as a function of pulsation phase have been detected interferometrically (Perrin et al. 1999; Thompson 2002; Thompson, Creech-Eakman & van Belle 2002). No single star in our sample has sufficient phase coverage for such a study. However, we have attempted to detect the pulsation by treating the sample



as a single “synthetic” Mira. A priori, the most promising approach appeared to be to explore this effect using the size ratios, due to their calibration advantages. However, as is apparent in Figure 2, no sinusoidal signature is present. We have also explored the possibility that the pulsation was not seen in the above approach due to the fact that instantaneous spectral type, rather than pulsation phase, might be the relevant parameter. Thus, we have used “phased spectral types” (column 4 of Table 5) from the literature (Terrill 1969; Lockwood & Wing 1971; Lockwood 1972) to search for a monotonic relation (also for the “synthetic Mira”) between the measured apparent sizes and the spectral type measured for the corresponding pulsation phase, also without success.

Forsaking the advantages of distance independence then, we show in Figure 3 our measured J/H/K’ linear sizes as a function of pulsation phase. As discussed by van Belle, Thompson & Creech-Eakman (2002), Hipparcos distances to Mira stars are rather uncertain, and therefore we have used distances from the literature based on period-luminosity (PL) relations, as indicated in Table 1. We note that we do not attempt to apply the PL relations using estimates of the absolute K-band magnitudes based on our own fringe data because the instrumentation and observing strategy were never intended for accurate photometry. Although the data errors are relatively large, and systematic deviations are apparent, the data suggests a sinusoidal signature with maximum sizes near phase = 0.5 (minimum light), as expected (as the photospheric size increases and cools, the star becomes fainter). The statistical significance of the sinusoidal signature is however marginal, with reduced  $\chi^2$  of 0.4, 0.8 and 0.9 at J/H/K’ respectively, compared with 1.9, 2.0 and 2.2 for models consisting of the constant average diameters. We note that while the observed sinusoid amplitudes (50 – 60% peak-to-peak) are comparable to those obtained from model predictions (Ireland, Scholz & Wood 2004), they are considerably larger than observed (9 – 26% peak-to-peak) when individual Miras are followed through their pulsation cycles (Thompson 2002; Thompson, Creech-Eakman & van Belle 2002). Also, it can be seen in Figure 3, that the linear sizes vary rather in unison, explaining why the pulsation was not apparent in the diameter ratios of Figure 2.

Ultimately, we believe that the failure to more convincingly detect the pulsation using the approaches just described is due to the fundamental inadequacy of those methods, as several physical mechanisms may contribute dispersion at levels comparable to the expected signatures: (a) intrinsic star-to-star differences, (b) our filters are broadband, and therefore probe a complex combination of emission from multiple layers of molecular gas just above the photosphere, with opacities which also change during the pulsation, making the true expected signature very complicated, and in particular potentially masking the photospheric layer motions (Ireland, Scholz & Wood 2004), and (c) some theoretical models predict cycle-to-cycle non-repeatability of the photospheric diameters, at significant levels (tens of %; Jacob

& Scholz 2002; Ireland, Scholz & Wood 2004), which if present would introduce that much dispersion in our apparent size vs. phase relations. On that last point, we note however that for the only published multi-cycle measurements to date (Thompson 2002; Thompson, Creech-Eakman & van Belle 2002) this effect was not observed; although it appears to be present (at 5 – 15% levels) in yet un-published data by the same group (Thompson R. R. 2004, private communication). In the literature, the success of the “synthetic” Mira method is mixed: while van Belle et al. (1996) saw a 20% peak-to-peak change in the effective temperatures of a sample of 18 Miras, the effect was not explored in the 22 star sample of their follow-up paper van Belle, Thompson & Creech-Eakman (2002), and appears not to be present by straightforward plotting of their published numbers. We finally note that the best case in our sample in which to search for a pulsation signature of an individual star (U Per, period = 320 days) was observed at two epochs almost exactly one cycle apart, and the measured UD sizes differ by 10, 12, and 6% at J, H and K' respectively, a marginally significant size change.

Several optical interferometers around the world are now equipped to measure accurate visibilities in broad or narrow spectral bands, and together span the visible to mid-infrared spectrum. Although recent efforts over more limited regions of the spectrum have clearly illustrated the power of multi-wavelength spatially resolved observations (Perrin et al. 2004; Jacob et al. 2004; Ohnaka 2004; Weiner 2004), global modelling fitting has however not been attempted to date, but represents the necessary next step toward a better theoretical understanding of Mira star atmospheres and dynamics.

The authors wish to acknowledge fruitful discussions with Robert Thompson, Gerard van Belle and Sam Ragland. This work has made use of services produced by the Michelson Science Center at the California Institute of Technology. This research has made use of the SIMBAD database, operated at CDS, Strasbourg, France. This research has made use of the NASA/ IPAC Infrared Science Archive, which is operated by the Jet Propulsion Laboratory, California Institute of Technology, under contract with the National Aeronautics and Space Administration. This research has made use of NASA’s Astrophysics Data System Service. E.P. wishes to acknowledge that part of this work was performed while he was a predoctoral fellow of the Smithsonian Astrophysical Observatory.

## REFERENCES

- Bessell, M. S., Brett, J. M., Wood, P. R. and Scholz, M., 1989, *A&A*, 213, 209
- Bonneau, D., Foy R. Blazit, A. and Labeyrie, A., 1982, *A&A*, 106, 235

- Bonneau, D. and Labeyrie, A., 1973, ApJ, 181, L1
- Borde, P., Coude du Foresto V., Chagnon G. and Perrin G. 2002, A&A, 393, 183-193
- Cohen M., Walker R.G., Carter B., Hammersley P., Kidger M. and Noguchi K., 1999, AJ, 117, 1864-1889
- Haniff, C. A., Scholz, M. and Tuthill, P. G., 1995, MNRAS, 276, 640
- Hofmann, K-H. , et al., 2003, in proceedings of the SPIE, “Interferometry for Optical Astronomy II, Ed. W. A. Traub, 4838, 1043
- Hofmann, K.-H., et al., 2002, New A, 7, 9
- Hofmann, K.-H., et al., 2001, A&A, 376, 518
- Hofmann, K.-H., et al., 2000, A&A, 353, 1016
- Ireland, M. J., Tuthill, P. G., Bedding, T. R., Robertson, J. G. and Jacob, A. P., 2004, MNRAS, 350, 365
- Ireland, M. J., Scholz, M. and Wood, P. R., 2004, MNRAS, 352, 318
- Jacob, A. P., Bedding, T. R., Robertson, J. G., Barton, J. R., Haniff, C. A. and Marson, R. G., 2004, MNRAS, 349, 303
- Jacob, A. P. and Scholz, M., 2002, MNRAS, 336, 1677
- Jura, M. and Kleinmann, S.G., 1992, ApJS, 79, 105
- Labeyrie, A., Koechlin, L. Bonneau, D. Blazit, A. Foy, R., 1977, ApJ, 218, L75
- Lockwood, G. W. and Wing, R. F., 1971, ApJ, 169, 63
- Lockwood, G. W., 1972, ApJS, 24, 375
- Lane B.F., Boden A.F., and Kulkarni S.R., 2001, ApJ, 551, L81-L83
- Monnier, J. D., et al., 2004, ApJ, 605, 436
- Mennesson, B. et al., 2002, ApJ, 579, 446
- Millan-Gabet R. 1999, PhD thesis, University of Massachusetts at Amherst
- Millan-Gabet R., Schloerb F. P., Traub W. A. and Carleton N. P. 1999, PASP, 111, 238

- Millan-Gabet R., Schloerb F. P., and Traub W. A. 2001, ApJ, 546, 358
- Ohnaka, K., 2004, A&A, 421, 1149
- Pauls, T., Young, J. S., Cotton, W. D., Monnier, J. D., 2004, to appear in proceedings of the SPIE, “New Frontiers in Stellar Interferometry”, Ed. W. A. Traub, 5491
- Perrin, G., et al., 2004, A&A, submitted
- Perrin, G., et al., 1999, A&A, 345, 221
- Richichi A. and Percheron, I., 2002, A&A, 386, 492
- Scholz, M., 2003, in proceedings of the SPIE, “Interferometry for Optical Astronomy II”, Ed. W. A. Traub, 4838, 163
- Scholz, M., 2001, MNRAS, 321, 347
- Terrill, C. L., 1968, AJ, 74, 413
- Thompson, R. R., 2002, PhD Thesis, University of Wyoming
- Thompson, R. R., Creech-Eakman, M. J. and van Belle, G. T., 2002, ApJ, 577, 447
- Traub W. A. 1998, in Proc. SPIE Vol. 3350, Astronomical Interferometry, ed. Robert D. Reasenberg, 848-855
- Tuthill, P. G., Monnier, J. D. and Danchi, W. C., 2000, Proc. SPIE, 4006, 491
- Tuthill, P. G., Danchi, W. C. Hale, D. S., Monnier, J. D. and Townes, C. H., 2000, ApJ, 534, 907
- Tuthill, P. G., Haniff, C. A., Baldwin, J. E., Feast, M. W., 1994, MNRAS, 266, 745
- van Belle G. T., Dyck H. M., Benson, J. A. and Lacasse, M. G., 1996, AJ, 112, 2147
- van Belle G. T., et al., 1997, AJ, 114, 2150
- van Belle G. T., 1999, PASP, 111, 1515
- Van Belle G.T., Ciardi D.R., Thompson R.R., Akeson R.L. and Lada E.A., 2001, ApJ, 559, 1155-1164
- van Belle, G. T., Thompson, R. R. and Creech-Eakman, M. J., 2002, AJ, 124, 1706

Weigelt, G., 2003, in proceedings of the SPIE, “Interferometry for Optical Astronomy II”,  
Ed. W. A. Traub, 4838, 181

Weiner, J., 2004, ApJ, 611, 37

Weiner, J., Hale, D. D. S. and Townes, C. H., 2003, ApJ, 589, 976

Weiner, J., Hale, D. D. S. and Townes, C. H., 2003, ApJ, 588, 1064

Wyatt, S.P., Cahn, J.H., 1983, ApJ, 275, 225

Young, K., 1995, ApJ, 445, 872

Table 1. Basic properties of Mira star sample.

Name	RA (J2000)	DEC (J2000)	$V_{min}-V_{max}$	J	H	K	Spectral Type	Distance (pc)	Distance reference
R And	00 24 01.95	+38 34 37.3	7 – 15	2.0	0.7	0.1	S	$532 \pm 101$	2
Z Cet	01 06 45.13	−01 28 52.9	9 – 14	4.6	3.7	3.3	M5	$920 \pm 175$	4
U Per	01 59 35.12	+54 49 20.0	8 – 12	2.2	1.2	0.9	M6	$559 \pm 140$	1
R Per	03 30 02.98	+35 40 17.1	9 – 14	4.8	4.0	3.2	M4	...	...
R Aur	05 17 17.69	+53 35 10.0	7 – 13	1.0	−0.1	−0.5	M7	$342 \pm 85$	1
S Ori	05 29 00.89	−04 41 32.7	8 – 14	0.9	−0.01	−0.5	M7	$481 \pm 120$	1
U Ori	05 55 49.17	+20 10 30.7	6 – 13	1.1	0.2	−0.3	M8	$310 \pm 77$	1
X Aur	06 12 13.38	+50 13 40.4	8 – 14	4.5	3.8	3.2	K2	...	...
R Cnc	08 16 33.83	+11 43 34.5	6 – 11	0.8	−0.3	−0.7	M7	$300 \pm 30$	5
R LMi	09 45 34.28	+34 30 42.8	8 – 13	1.7	0.5	−0.1	M7	$367 \pm 22$	1
R Leo	09 47 33.49	+11 25 43.6	6 – 10	−0.7	−1.7	−2.3	M8	$115 \pm 29$	1
R Hya	13 29 42.78	−23 16 52.8	5 – 8	−1.3	−2.2	−2.7	M7	$110 \pm 21$	4
W Hya	13 49 02.00	−28 22 03.5	6 – 9	−1.7	−2.6	−3.2	M7	$80 \pm 15$	4
S Crb	15 21 23.96	+31 22 02.6	7 – 13	1.1	0.2	−0.2	M7	$375 \pm 94$	1
RS Lib	15 24 19.79	−22 54 39.9	7 – 13	1.0	−0.1	−0.6	M	$210 \pm 40$	3
R Ser	15 50 41.73	+15 08 01.1	6 – 14	1.3	0.4	0.1	M7	$356 \pm 89$	1
S Her	16 51 53.92	+14 56 30.8	6 – 13	2.3	1.2	1.0	M6	$677 \pm 169$	1
Ry Lyr	18 44 51.9	+34 40 30.0	10 – 15	...	...	...	M6	...	...
R Aql	19 06 22.2	+08 13 48.0	6 – 12	0.7	−0.3	−0.8	M7	$224 \pm 56$	1
R Peg	23 06 39.2	+10 32 36.1	7 – 13	1.8	0.9	0.4	M7	$435 \pm 109$	1
W Peg	23 19 50.5	+26 16 43.7	8 – 13	1.1	0.2	−0.1	M7	$310 \pm 31$	5
S Peg	23 20 32.6	+08 55 08.1	8 – 13	2.3	1.4	1.0	M6	$675 \pm 169$	1

Table 1—Continued

Name	RA (J2000)	DEC (J2000)	$V_{min}-V_{max}$	J	H	K	Spectral Type	Distance (pc)	Distance reference
R Aqr	23 43 49.5	-15 17 04.2	6.5 - 11	-0.1	-1.1	-1.6	M7	$272 \pm 68$	1

Note. — V magnitudes and spectral types are from the AAVSO and SIMBAD databases, near-infrared magnitudes are from the 2MASS database; as these stars are by definition variable, this information is meant to be merely representative.

References. — (1) van Belle, Thompson & Creech-Eakman (2002); (2) van Belle et al. (1997); (3) Young (1995); (4) Jura & Kleinmann (1992); (5) Wyatt & Cahn (1983)

Table 2. Log of observations.

Name	Date (yy/mm/dd)	Julian Date (−2450000)	Baseline	Filters	Calibrator(s)
R And	97/11/21	0774.0	S15N35	H/K'	HR82, HR175
Z Cet	98/11/04	1122.0	S15N35	J/H/K'	HR353
U Per	97/11/19	0772.0	S15N35	J/H/K'	HR787
U Per	98/10/01	1088.0	S15N35	J/H/K'	HR470
R Per	98/10/02	1089.0	S15N35	J/H/K'	HR876
R Per	98/11/05	1123.0	S15N35	J/H/K'	HR876
R Aur	97/10/12	0734.0	S15N15	J/H	HR1866
R Aur	97/11/19	0772.0	S15N35	H/K'	HR1588, HR1866
R Aur	97/11/22	0775.0	S15N35	H/K'	HR1588
S Ori	98/11/05	1123.0	S15N35	H/K'	HR1830
U Ori	97/10/17	0739.0	S15N15	J/H	HR2169
U Ori	97/11/21	0774.0	S15N35	K'	HR2047
U Ori	97/11/23	0776.0	S15N35	H/K'	HR2047
X Aur	97/10/14	0736.0	S15N15	J/H/K'	HR2338
R Cnc	98/03/02	0875.0	S15N15	H/K'	HR2864
R Lmi	97/11/20	0773.0	S15N35	K'	HR3791
R Lmi	98/02/28	0873.0	S15N15	J/H/K'	HR4081
R Lmi	98/03/02	0875.0	S15N15	J/H/K'	HR4081
R Leo	98/03/01	0874.0	S15N15	H/K'	HR3877
R Hya	98/02/28	0873.0	S15N15	J/H/K'	HR5020, HR4958
R Hya	98/03/02	0875.0	S15N15	J/H/K'	HR5020, HR4958
W Hya	98/03/01	0874.0	S15N15	H/K'	HR5312
S Crb	98/03/01	0874.0	S15N15	J/H/K'	HR5674
S Crb	98/06/12	0977.0	S15N35	H/K'	HR5674
RS Lib	98/02/28	0873.0	S15N15	J/H/K'	HR5824
R Ser	98/03/02	0875.0	S15N15	J/H/K'	HR5940
R Ser	98/03/07	0880.0	S15N35	H/K'	HR5940
S Her	98/06/15	0980.0	S15N35	J/H	HR6542, HR6065
Ry Lyr	98/06/15	0980.0	S15N35	H/K'	HR7192
R Aql	98/06/13	0978.0	S15N35	H/K'	HR7557



Table 2—Continued

Name	Date (yy/mm/dd)	Julian Date (−2450000)	Baseline	Filters	Calibrator(s)
R Peg	98/10/01	1088.0	S15N35	J/H/K'	HR8608
W Peg	98/10/01	1088.0	S15N35	H/K'	HR9051
S Peg	98/09/30	1087.0	S15N35	J/H/K'	HR8916
R Aqr	97/10/17	0739.0	S15N15	J/H/K'	HR8980

Note. — The baseline designations are as follows: SxNy refers to South telescope being at the x meter station and the North telescope at the y meter station. The [length,azimuth] of the S15N15 and S15N35 baselines are [21 m,−3.8 deg] and [38 m,+18 deg] respectively.

Table 3. Calibrator estimated diameters and uncertainties.

Calibrator (HR number)	Calibrator (HD number)	Spectral Type	Angular Diameter (mas)	Reference
HR82	HD1671	F5III	$0.65 \pm 0.08$	1a
HR175	HD3817	G8III	$1.19 \pm 0.15$	3
HR353	HD7147	K4III	$1.59 \pm 0.20$	3
HR470	HD10110	K5III	$1.84 \pm 0.02$	2
HR787	HD16735	K0II	$1.29 \pm 0.16$	3
HR876	HD18339	K3III	$1.45 \pm 0.18$	3
HR978	HD20277	G8IV	$1.14 \pm 0.09$	4
HR1133	HD23193	A2m	$0.23 \pm 0.04$	4
HR1588	HD31579	K4III	$1.78 \pm 0.23$	3
HR1698	HD33856	K3III	$2.13 \pm 0.02$	1b
HR1830	HD36134	K1III	$1.29 \pm 0.16$	3
HR1866	HD36678	M0III	$2.55 \pm 0.03$	2
HR2047	HD39587	G0V	$1.11 \pm 0.20$	4
HR2105	HD40486	K0	$1.87 \pm 1.33$	4
HR2169	HD42049	K4III	$2.17 \pm 0.28$	3
HR2188	HD42466	K1III	$0.96 \pm 0.12$	3
HR2338	HD45466	K4III	$2.17 \pm 0.28$	3
HR2864	HD59294	K1III	$2.24 \pm 0.03$	2
HR3115	HD65522	K2	$1.50 \pm 0.98$	4
HR3319	HD71250	M3III	$4.61 \pm 0.60$	3
HR3791	HD82522	K4III	$1.13 \pm 0.14$	3
HR3877	HD84561	K4III	$2.15 \pm 0.27$	3
HR4081	HD90040	K1III	$1.48 \pm 0.19$	3
HR4958	HD114149	K0III	$1.51 \pm 0.19$	3
HR5020	HD115659	G8III	$3.27 \pm 0.41$	3
HR5228	HD121156	K2III	$0.96 \pm 0.12$	3
HR5312	HD124206	K3III	$1.78 \pm 0.22$	3
HR5674	HD135438	K5	$2.57 \pm 2.70$	4
HR5824	HD139663	K3III	$1.99 \pm 0.02$	2
HR5940	HD142980	K1IV	$1.27 \pm 0.16$	3

Table 3—Continued

Calibrator (HR number)	Calibrator (HD number)	Spectral Type	Angular Diameter (mas)	Reference
HR6065	HD146388	K3III	$1.22 \pm 0.15$	3
HR6542	HD159353	K0III	$1.10 \pm 0.14$	3
HR6770	HD165760	G8III	$1.74 \pm 0.22$	3
HR6793	HD166229	K2III	$1.56 \pm 0.20$	3
HR7192	HD176670	K3III	$2.33 \pm 0.03$	2
HR7557	HD187642	A7V	$3.25 \pm 0.41$	1c
HR7804	HD194258	M5III	$6.62 \pm 0.87$	3
HR8608	HD214298	K5	$1.77 \pm 0.87$	4
HR8916	HD220954	K1III	$1.94 \pm 0.02$	2
HR8961	HD222107	G8III	$2.64 \pm 0.33$	3
HR8980	HD222547	K4III	$2.73 \pm 0.35$	3
HR8987	HD222643	K3III	$2.00 \pm 0.25$	3
HR9010	HD223173	K3II	$2.48 \pm 0.32$	3
HR9029	HD223559	K4III	$2.15 \pm 0.27$	3
HR9051	HD224128	K5	$1.49 \pm 0.55$	4

References. — (1) from CHARM catalog (Richichi & Percheron 2002); (1a) Lane, Boden & Kulkarni (2001); (1b) Cohen et al. (1999); (1c) van Belle et al. (2001); (2) Borde et al. (2002); (3) van Belle (1999); (4) *getCal/Fbol*

Table 4. Calibrated visibility data.

Name	Date (yymmdd)	Julian Date	Filter	$u$ ( $arcsec^{-1}$ )	$v$ ( $arcsec^{-1}$ )	Visibility Amplitude
R And	971121	2450774	H	-2.22	112.25	$0.463 \pm 0.035$
R And	971121	2450774	H	-4.79	112.16	$0.419 \pm 0.035$
R And	971121	2450774	H	-12.91	111.48	$0.485 \pm 0.035$
R And	971121	2450774	K'	-13.46	83.05	$0.766 \pm 0.040$
R And	971121	2450774	K'	-15.92	82.57	$0.712 \pm 0.040$
Z Cet	981104	2451122	J	57.79	118.31	$0.858 \pm 0.026$
Z Cet	981104	2451122	J	54.73	118.25	$0.850 \pm 0.026$
Z Cet	981104	2451122	J	51.98	118.19	$0.863 \pm 0.026$
Z Cet	981104	2451122	H	52.04	89.86	$0.858 \pm 0.021$
Z Cet	981104	2451122	H	50.23	89.80	$0.843 \pm 0.021$
Z Cet	981104	2451122	H	48.24	89.74	$0.838 \pm 0.021$
Z Cet	981104	2451122	K'	26.08	67.09	$0.913 \pm 0.010$
Z Cet	981104	2451122	K'	24.98	67.07	$0.918 \pm 0.010$
U Per	971119	2450772	J	-10.34	140.05	$0.509 \pm 0.022$
U Per	971119	2450772	J	-14.74	139.53	$0.515 \pm 0.022$

Note. — The complete version of this table is in the electronic edition of the Journal. The printed edition contains only a sample. The complete data set is also available in the OI-FITS format (Pauls et al. 2004) upon request.

Table 5. Near-infrared angular diameters and diameter ratios.

Name	Julian Date (-245000)	Phase	Phased Spectral Type (M subclass)	$D_J$ (mas)	$D_H$ (mas)	$D_K$ (mas)	$R_{J/H}$	$R_{H/K}$
R And	0774.0	0.6	6.0	...	$6.6 \pm 0.2$	$5.7 \pm 0.3$	...	$1.16 \pm 0.07$
Z Cet	1122.0	0.25	5.0	$2.7 \pm 0.2$	$3.5 \pm 0.2$	$3.7 \pm 0.2$	$0.76 \pm 0.05$	$0.95 \pm 0.06$
U Per	0772.0	0.8	6.0	$5.0 \pm 0.1$	$5.4 \pm 0.1$	$6.6 \pm 0.2$	$0.93 \pm 0.02$	$0.83 \pm 0.03$
U Per	1088.0	0.9	5.5	$4.5 \pm 0.1$	$4.85 \pm 0.05$	$5.0 \pm 0.3$	$0.93 \pm 0.01$	$0.97 \pm 0.05$
R Per	1089.0	0.3	6.3	$< 1.6$	$< 0.9$	$< 2.7$	...	...
R Per	1123.0	0.5	7.5	$< 1.5$	$< 2.2$	$< 1.8$	...	...
R Aur	0734.0	0.7	8.5	$11.1 \pm 0.1$	$10.5 \pm 0.3$	...	$1.05 \pm 0.03$	...
R Aur	0772.0	0.8	8.5	...	$9.3 \pm 0.1$	$10.1 \pm 0.1$	...	$0.92 \pm 0.01$
R Aur	0775.0	0.8	8.5	...	$9.2 \pm 0.1$	$10.1 \pm 0.1$	...	$0.91 \pm 0.01$
S Ori	1123.0	0.1	6.3	...	$9.1 \pm 0.1$	$9.6 \pm 0.2$	...	$0.95 \pm 0.02$
U Ori	0739.0	0.9	9.0	$10.9 \pm 0.1$	$12.5 \pm 0.1$	...	$0.87 \pm 0.01$	...
U Ori	0774.0	0.04	8.2	$11.5 \pm 0.1$	...	...	...	...
U Ori	0776.0	0.04	8.2	...	$9.2 \pm 0.3$	$10.5 \pm 0.4$	...	$0.87 \pm 0.05$
X Aur	0736.0	0.1	3.4	$< 3.3$	$< 3.2$	$< 5.2$	...	...
R Cnc	0875.0	0.4	7.5	...	$15.3 \pm 0.2$	$18.9 \pm 0.2$	...	$0.81 \pm 0.01$
R LMi	0773.0	0.2	8.0	...	...	$12.1 \pm 0.1$	...	...
R LMi	0873.0	0.5	9.0	$12.5 \pm 0.1$	$12.8 \pm 0.2$	$14.2 \pm 0.2$	$0.97 \pm 0.01$	$0.91 \pm 0.02$
R LMi	0875.0	0.5	9.0	$12.6 \pm 0.1$	$13.5 \pm 0.1$	$14.7 \pm 0.1$	$0.94 \pm 0.01$	$0.91 \pm 0.01$
R Leo	0874.0	0.4	7.5	...	$23.8 \pm 0.3$	$29.91 \pm 0.27$	...	$0.79 \pm 0.01$
...	...	...	...	...	$32.4 \pm 0.4$	...	...	...
R Hya	0873.0	0.8	8.0	$19.8 \pm 1.1$	$22.7 \pm 0.6$	$23.9 \pm 0.5$	$0.87 \pm 0.05$	$0.95 \pm 0.03$

Table 5—Continued

Name	Julian Date (-245000)	Phase	Phased Spectral Type (M subclass)	$D_J$ (mas)	$D_H$ (mas)	$D_K$ (mas)	$R_{J/H}$	$R_{H/K}$
R Hya	0875.0	0.8	8.0	$20.5 \pm 0.2$	$22.0 \pm 0.4$	$25.8 \pm 0.2$	$0.93 \pm 0.02$	$0.86 \pm 0.01$
W Hya	0874.0	0.6	7.0	...	$31.2 \pm 0.3$	$39.9 \pm 0.2$	...	$0.78 \pm 0.01$
S Crb	0874.0	0.4	7.5	$9.2 \pm 0.7$	$8.9 \pm 0.9$	$9.2 \pm 0.9$	$1.04 \pm 0.13$	$0.96 \pm 0.14$
S Crb	0977.0	0.6	9.0	...	$9.1 \pm 0.5$	$11.2 \pm 0.4$	...	$0.81 \pm 0.05$
RS Lib	0873.0	1.0	7.5	$9.8 \pm 0.4$	$9.1 \pm 0.9$	$9.3 \pm 1.1$	$1.08 \pm 0.11$	$0.98 \pm 0.15$
R Ser	0875.0	0.0	4.0	$7.5 \pm 0.1$	$8.3 \pm 0.7$	$10.4 \pm 0.4$	$0.90 \pm 0.07$	$0.80 \pm 0.07$
R Ser	0880.0	0.1	6.0	...	$6.8 \pm 0.1$	$7.9 \pm 0.1$	...	$0.86 \pm 0.01$
S Her	0980.0	0.6	8.0	$5.4 \pm 0.3$	$5.6 \pm 0.2$	...	$0.97 \pm 0.06$	...
Ry Lyr	0980.0	0.35	7.7	...	$2.7 \pm 0.3$	$< 2.03$	...	...
R Aql	0978.0	0.9	7.5	...	$9.3 \pm 0.1$	$10.6 \pm 0.1$	...	$0.88 \pm 0.01$
R Peg	1088.0	0.0	7.0	$6.0 \pm 0.4$	$7.0 \pm 0.3$	$9.6 \pm 0.2$	$0.86 \pm 0.06$	$0.73 \pm 0.03$
W Peg	1088.0	0.1	6.9	...	$8.2 \pm 0.1$	$9.6 \pm 0.1$	...	$0.86 \pm 0.01$
S Peg	1087.0	0.1	5.2	$3.9 \pm 0.1$	$4.9 \pm 0.3$	$4.8 \pm 0.5$	$0.79 \pm 0.05$	$1.02 \pm 0.12$
R Aqr	0739.0	0.4	7.5	$17.7 \pm 0.2$	$17.7 \pm 0.1$	$20.8 \pm 0.8$	$1.00 \pm 0.01$	$0.85 \pm 0.03$

Note. — For R Leo, the two H-band diameter values indicated correspond to the two possible solutions that exist in the second lobe of the visibility function, see § 4 for discussion.

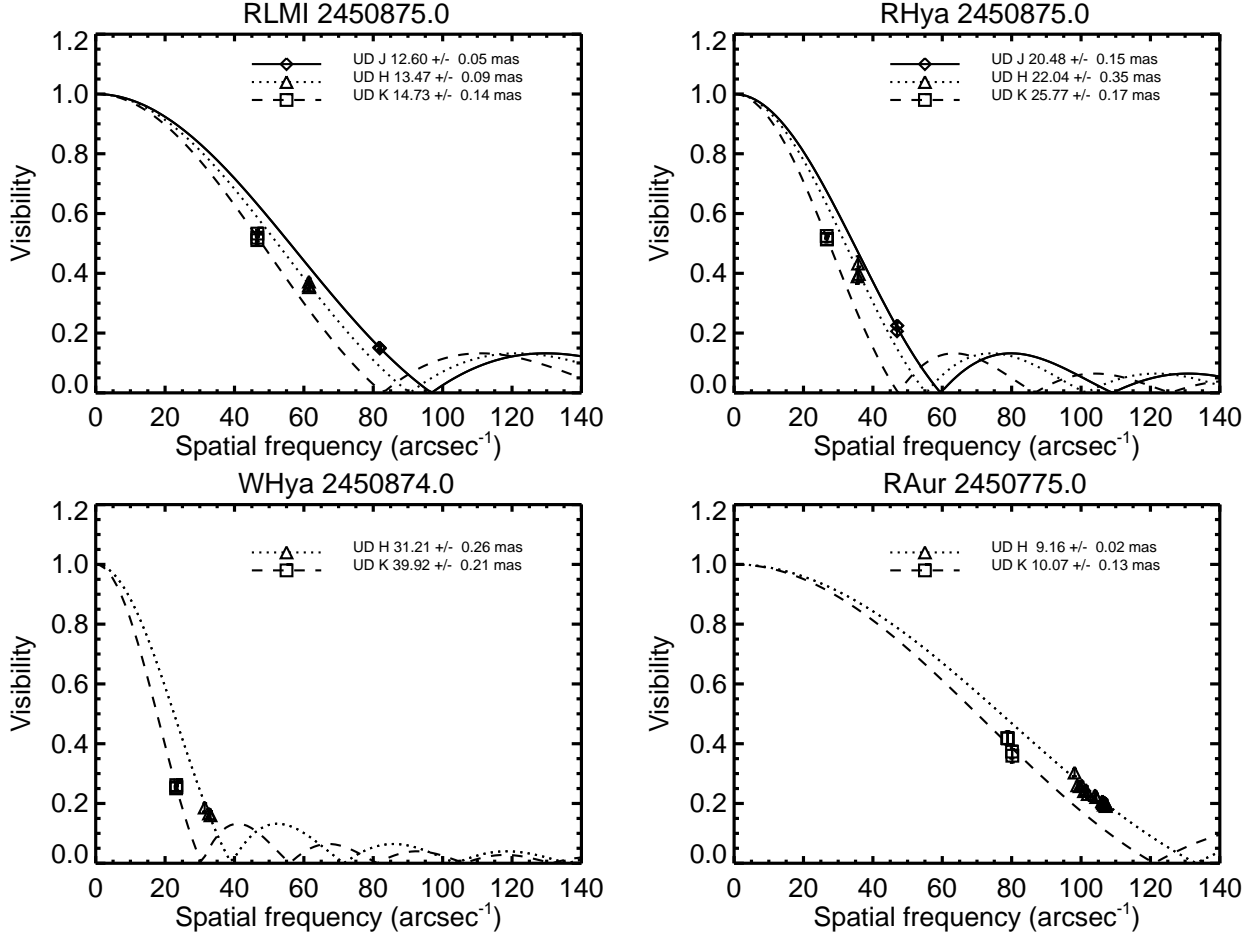


Fig. 1.— Example visibility data. The four panels illustrate the general finding that lower visibilities are measured at the longer near-infrared wavelengths (J diameter < H diameter < K' diameter). The bottom-right panel also illustrates the data precision. In all panels, the abscissa is the spatial frequency given by the projected baseline  $B_p/\lambda_0 = \sqrt{u^2 + v^2}$ ; and the ordinate is the visibility amplitude (1.0 for a point-like source, 0.0 for a completely resolved extended source).

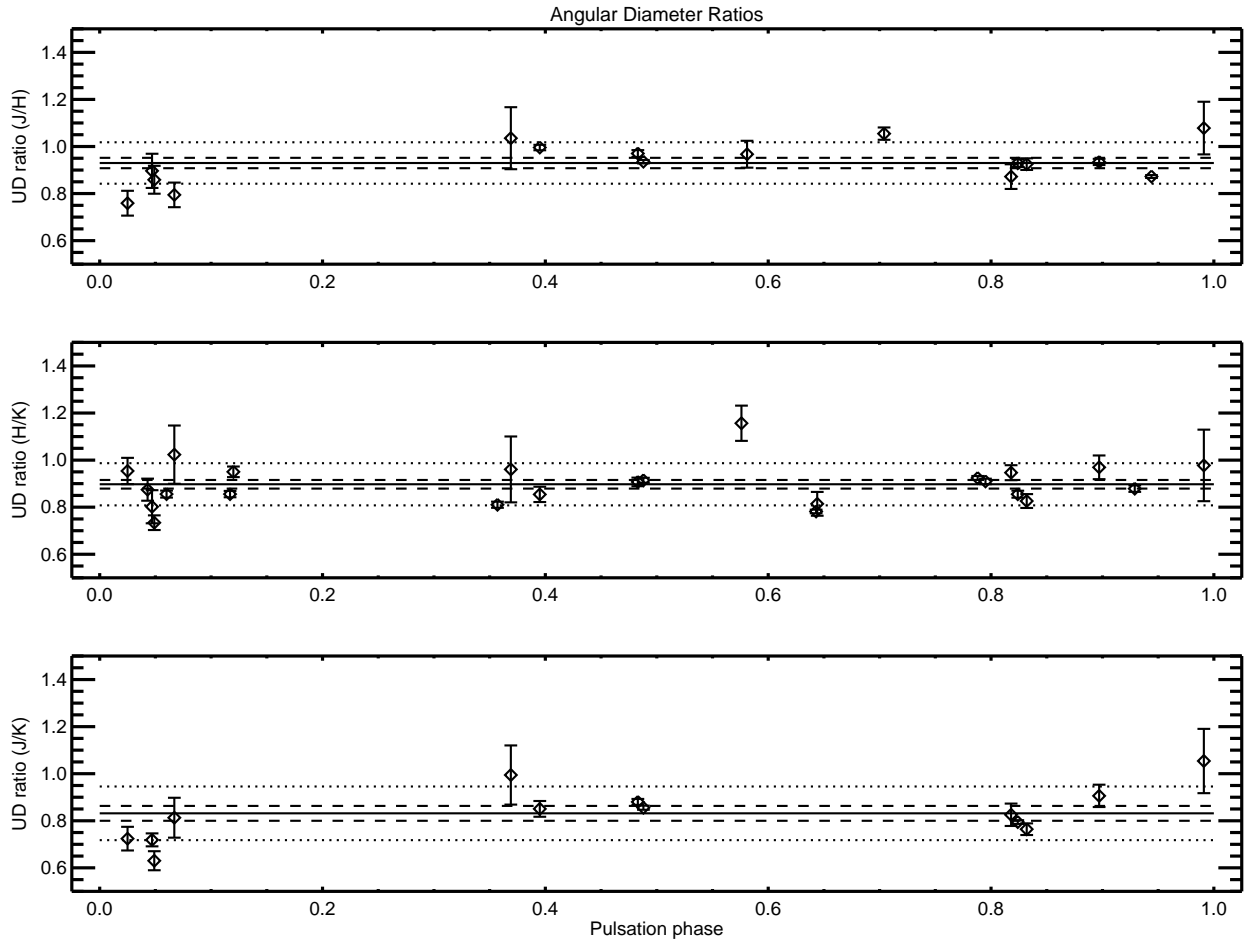


Fig. 2.— Angular diameter ratios. For each panel, the solid line indicates the measured mean ratio, the dashed lines indicate the error in the mean, and the dotted lines indicate the RMS of the sample.



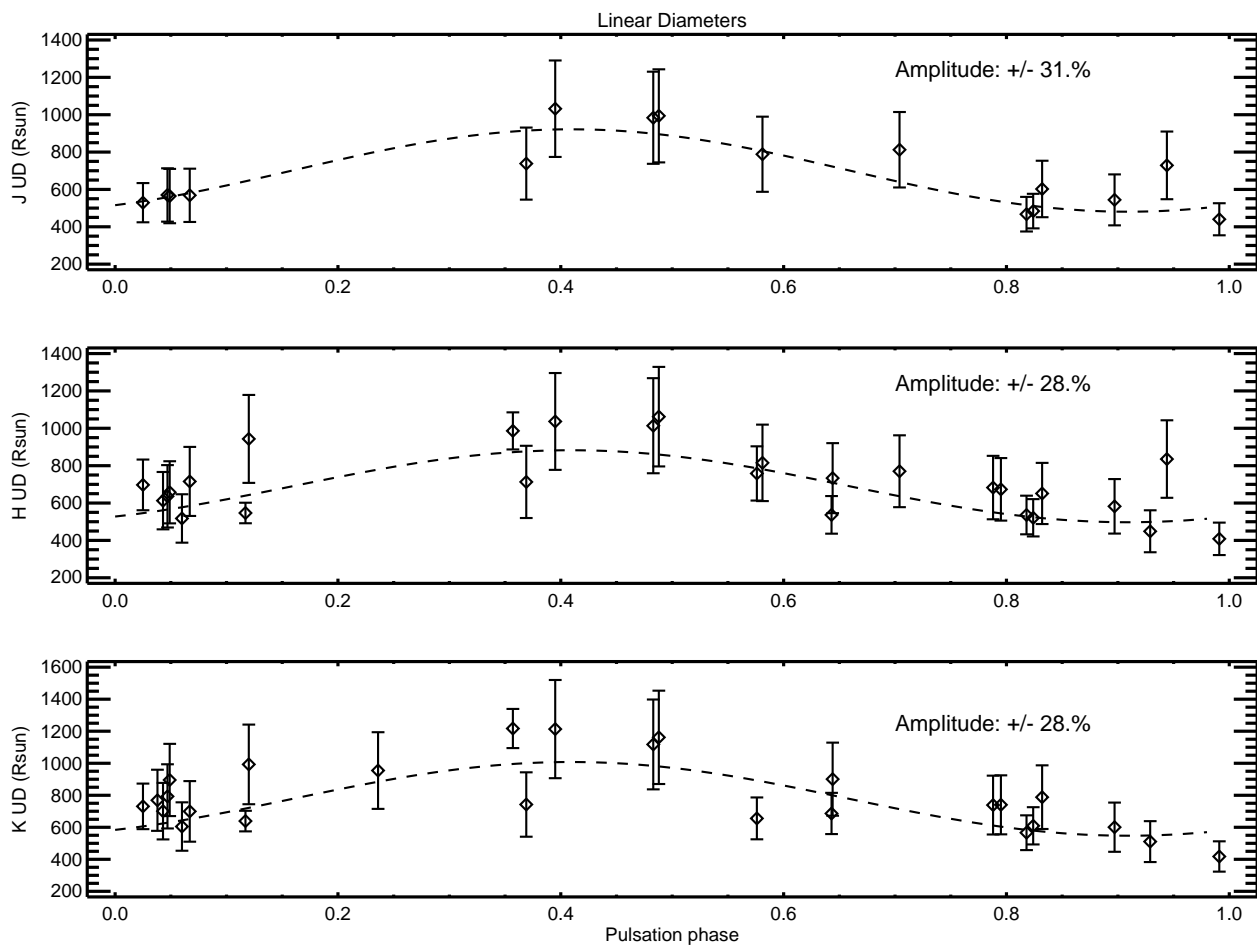


Fig. 3.— Linear diameters as a function of pulsation phase. In each panel, the dashed line indicates a sinusoidal fit to the data. The sinusoidal fits have 4 free parameters: mean, amplitude, period and phase; except for the  $K'$ -band data, where we fix the period and phase to the values found in the J and H fits. See § 5 for discussion.